Nanoparticle Field Extraction Thruster (nanoFET): Design and Results of the Microparticle Emitter Prototype

IEPC-2007-80

Presented at the 30th International Electric Propulsion Conference, Florence, Italy
September 17-20, 2007

Louis Musinski[*], Thomas Liu[†], Brian Gilchrist[‡], Alec Gallimore[§], and *Michael Keidar*[**]
University of Michigan, Ann Arbor, MI 48109

Abstract: **This paper presents the design and results from the first generation microparticle emitter prototype developed at the University of Michigan. This prototype was designed to further the understanding of the physics governing the nanoparticle Field Extraction Thruster (nanoFET) concept. The nanoFET concept proposes an electric propulsion approach that can have a highly adjustable charge-to-mass ratio and electrostatic acceleration that potentially could span a specific impulse range from ~100 s to ~10,000 s and thrust power ranging from microwatts to many tens of kilowatts at high efficiency. Here, we present experimental results from spherical and cylindrical particle extraction tests from an insulating liquid. Using the prototype, we have successfully demonstrated the extraction of particles with diameters as small as a few tens of microns. In addition, this paper investigates potential issues with the first generation prototype and makes suggestions for the development of future generations.**

Nomenclature

A	= cross-sectional area of particle [m^2]	ε_o	= permittivity of free space [F/m]
β	= aspect ratio of cylindrical particle	ε_l	= permittivity of liquid [F/m]
C_e	= constant taking value of 1.34 – 4.5	F_s	= surface tension force [N]
d	= electrode gap width [m]	g	= gravitational constant [m/s^2]
d_{ch}	= height of charging gap [m]	γ	= surface tension [N/m]
d_{ex}	= height of extraction gap [m]	Isp	= specific impulse [s]
d_{liq}	= height of liquid [m]	r	= radius of particles [m]
δ	= liquid thickness coating particle [m]	R	= radius of liquid perturbation [m]
E_{ch}	= charging electric field [V/m]	ρ_l	= density of liquid [kg/m^3]
E_{ex}	= extraction electric field [V/m]	ρ_p	= density of particle [kg/m^3]
$E_{ex,thresh,sph}$	= spherical extraction electric field [V/m]	V_{ch}	= charging potential [V]
$E_{ex,thresh,cyl}$	= cylindrical extraction electric field [V/m]	V_{ex}	= extraction potential [V]
$E_{liq,thresh}$	= liquid instability electric field [V/m]		

[*] Graduate Student, Electrical Engineering, louisdm@umich.edu
[†] Graduate Student, Aerospace Engineering, liutm@umich.edu
[‡] Professor, Electrical Engineering & Space Systems, gilchrst@umich.edu
[§] Arthur F. Thurnau Professor, Aerospace Engineering & Applied Physics, rasta@umich.edu
[**] Research Professor, Aerospace Engineering, Currently Assistance Professor, Mechanical and Aerospace Engineering, The George Washington University, keidar@gwu.edu

I. Introduction

The nanoparticle field extraction thruster, termed nanoFET, is under development at the University of Michigan. This new electrostatic thruster technology appears feasible using nanoparticles as propellant and utilizing micro- and nano-electromechanical systems (NEMS/MEMS) to transport, charge, extract, and accelerate the nanoparticles.[1,2]

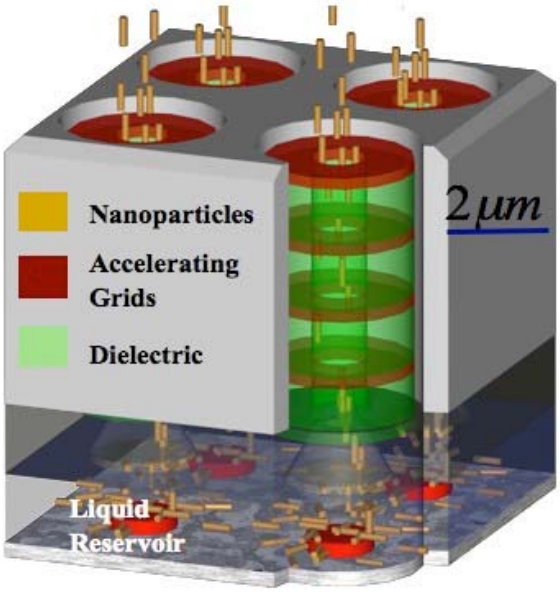

Figure 1: Schematic showing four nanoparticle emitters.

Figure 1 is a drawing of four identical nanoparticle emitters used in the MEMS/NEMS based nanoFET thruster concept where a multi-layer grid establishes the critical electric fields to charge, extract, accelerate, and eject conducting nanoparticles (examples shown in Figure 2)[3] from the surface of an insulating liquid used to transport these particles. These nanoparticles will likely have diameters ranging from 1 nm to over 10 nm and aspect ratios as high as 1,000.

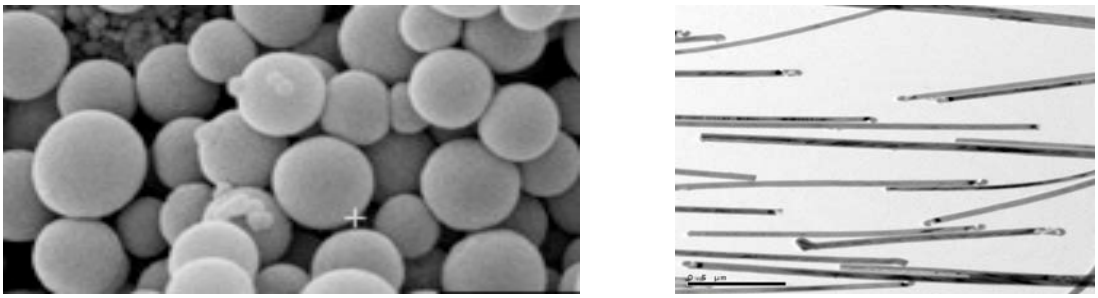

Figure 2: Example of a collection of unsorted nanoparticle spheres in the 10 nm diameter range (left) and cylinders with a diameter of 45 μm and length of 500 μm.

To understand how nanoFET works, Figure 3 depicts a functional schematic of a single emission zone from the nanoparticle thruster using an insulating liquid. The nanoparticles are initially housed in a low vapor pressure liquid-filled storage reservoir. These nano-spheres or cylinders would then be transported through a microfluidic transport system to emission zones. These zones are comprised of multiple layers of stacked electrodes with millions of micron-sized channels for particle acceleration. Beneath the accelerating channels are electrical charging pads that are submersed in the low vapor pressure liquid. The layers of stacked electrodes and the charging pads are electrically biased to produce strong electric fields in the accelerating channels and within the liquid reservoir.

Particles delivered to the emission zones through the microfluidic transport system become electrically charged when they contact one of the charging pads. After acquiring sufficient charge, the particles are transported by the electric field to the liquid surface, extracted through the surface, accelerated in the channels, and finally ejected to produce thrust

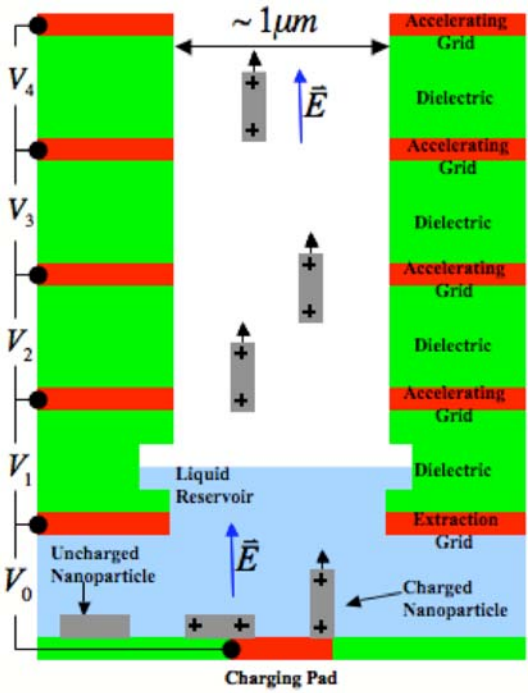

Figure 3: Cross-section schematic of a single emission channel used in the microparticle emitter prototype.

Using nanoparticles as opposed to ions or charged liquid droplets may provide many operational advantages, including the following:[4,5]

- *Enormous specific impulse range at high thrust efficiency:* The ability to tune propulsion characteristics via different nanoparticle dimensions and charge states has the potential of permitting thrust efficiencies over 80% for a specific impulse range of 100 s to 10,000 s. Such high efficiencies could result in high thrust-to-power ratios, especially at low specific impulse. Consequently, a nanoFET thruster could operate at high specific impulse in cruise mode and yet switch to a high thrust and low Isp mode when needed. This flexibility provides a wider margin for mission designers to accommodate off-nominal mission scenarios as well as dynamic re-tasking of space assets to take advantage of in-flight opportunities.

For example, by using just three types of nanoparticles made from carbon nanotubes (CNT), the nanoFET system should be capable of spanning an approximate Isp range from 150 s to 10,000 s. These three possible carbon nanotube particles are listed in Table 1.

Diameter [nm]	Length [μm]	Isp range [s]
16	3	150-750
4	3	750-2,700
1	3	2,700-10,000

Table 1: Carbon nanotube particles enabling nanoFET to span 150-10,000 second range.

Figure 4 shows a plot of nanoFET's expected thrust efficiency when using these three particles as a function of specific impulse.[6] Such performance can be obtained at reasonable acceleration voltages between 500 to 10,000 V due to the MEMS gated structures that provide the extraction and acceleration electric fields. Note that in the nanoFET system, efficiency losses may be due to viscous drag in the liquid, charge loss to the liquid, particle

impingement on the gates, and beam defocusing. Also included is a 5% inefficiency in the power system.

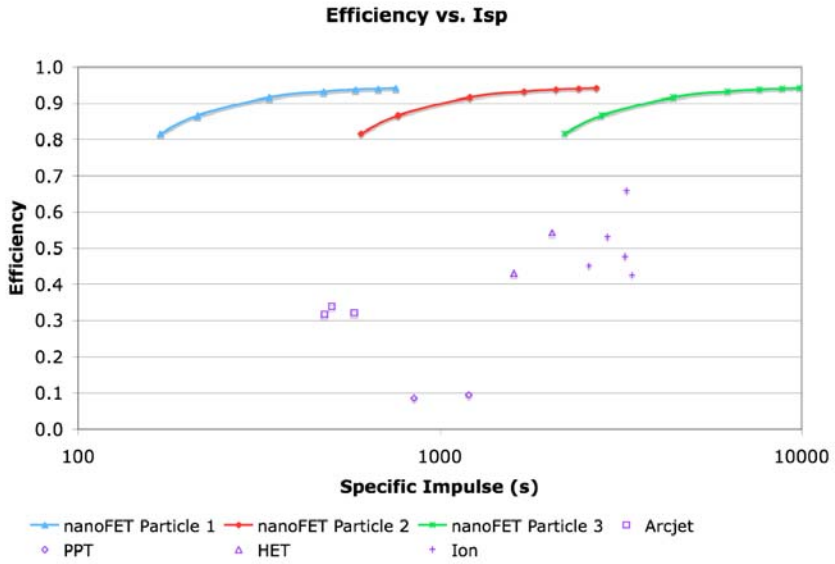

Figure 4: Possible efficiency performance of nanoFET for specific impulse range compared with other electric propulsion systems. The nanoparticles are specified in Table 1.

NanoFET's thrust-to-power performance compared to other state-of-the-art thruster types is shown in Figure 5. This level of performance could provide mission designers with the flexibility to engage a high thrust mode to climb out of gravity wells, perform abort scenarios or emergency maneuvers, and reduce trip times.

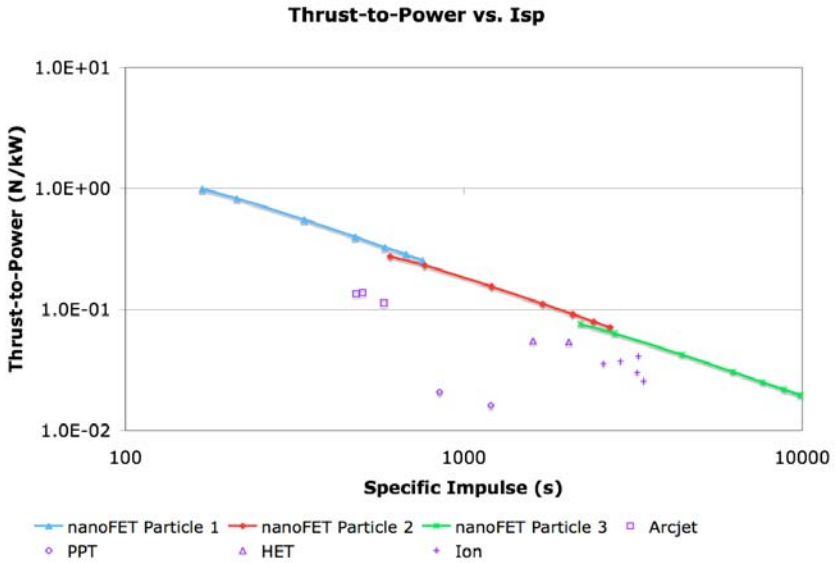

Figure 5: High thrust-to-power ratio for nanoFET compared to other electric propulsion systems. The nanoparticles are specified in Table 1.

- *Highly integrated system*: The use of MEMS technology enables a "flat panel" thruster design that incorporates power processing as well as nanoparticle manufacture, storage, feed, extraction, and acceleration. Such compact design simplifies propulsion system integration and lowers thruster specific mass. Because different regions of nanoFET can emit particles of opposite polarity, neutralizer requirements are simplified as nanoFET is a self-neutralizing thruster.

- *Geometrically scalable*: A "flat panel" design allows the nanoFET array size to be scalable with power, thus permitting a single ground qualified engine type to be used in applications ranging from nanosatellites operating at a few watts to space tugs or space stations in the hundreds of kilowatts range. Such "plug-and-play" functionality provides greater spacecraft design flexibility and significant cost savings.
- *Longer operational lifetime*: Charging of the nanoparticles is accomplished without ionization, meaning greater reliability and the absence of cathodes and charge exchange collisions that are the principal lifetime limiters of current electric propulsion systems. Propellant charging, as opposed to propellant ionizing, also accounts for part of the efficiency gains nanoFET affords.

II. Particle Extraction Utilizing the First Generation Microparticle Emitter Prototype

The development of the nanoparticle field extraction thruster (nanoFET) at the University of Michigan has focused on developing an understanding of the physics governing the particle charging, extraction, and acceleration processes. To simplify the process and increase the rate of knowledge development, most experiments have been conducted with particles ranging from many hundreds of microns to a few millimeters in size. Significant advances in the understanding of the physics have been made and we believe it is now important to begin scaling down the particle size to explore how the governing physics changes and to prove the feasibility of particle charging, extraction, and acceleration when using smaller particles.

While the ultimate goal is to demonstrate particle charging, extraction, and acceleration at the nanometer range, we believe that it is important to meet an intermediate goal of operating with particles ranging from microns to tens of microns in size. In addition, micron sized particles may prove to be useful for terrestrial applications such as material processing, printing, and biomedicine. To meet this goal, we have designed, fabricated, and tested the first generation microparticle emitter prototype, which is the focus of the remainder of this paper.

A. Decoupling of the Charging and Extraction Electric Fields

Before discussing the design of and results from the microparticle emitter prototype, this section will discuss the need for a new emitter system. Initial experiments demonstrated particle extraction with particles ranging from many hundreds of microns to a few millimeters in size by utilizing a dual electrode extractor as shown in Figure 6, where a potential bias was applied between the two electrodes to generate strong electric fields in the partially liquid filled electrode gap. The electric field within the liquid, E_{ch}, will be termed the charging electric field and is primarily responsible for charging the conducting particles when they are in contact with the bottom electrode. In addition to charging the particles, the charging field must transport the particles from the bottom electrode to the liquid surface. The electric field in the air/vacuum region, E_{ex}, will be termed the extraction electric field and is primarily responsible for extracting the charged particles through the liquid surface once they are delivered by the charging field. The extraction electric field is also responsible for the initial acceleration of the particles once they are extracted.

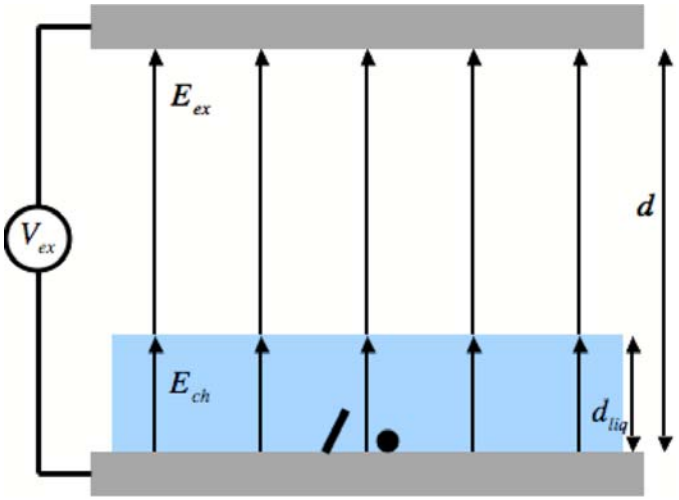

Figure 6: Experimental setup for particle extraction from an insulating liquid using a duel electrode extractor.

The use of this experimental setup successfully proved that both spherical and cylindrical particles could be charged, transported, extracted, and accelerated from an insulating liquid by applying high strength electric fields in both the liquid and air gaps. The minimum required extraction electric field to achieve particle extraction was previously derived for spherical and cylindrical particles to be[7]

$$E_{ex,thresh,sph} = \sqrt{\frac{3\gamma(r+\delta) + g\left[(r+\delta)^3\rho_\ell + 2r^3(\rho_p - \rho_\ell)\right]}{\pi^2 r^2 \varepsilon_o}} \text{ and} \tag{1}$$

$$E_{ex,thresh,cyl} = \sqrt{\frac{\left[\gamma(r+\delta) + g\beta\left\{r^3\rho_p - \rho_\ell\left(r^3 - \frac{(r+\delta)^3}{2\beta}\right)\right\}\right]\left[\ln(4\beta) - 1\right]}{2r^2\beta^2\varepsilon_o}}\ , \tag{2}$$

respectively, where r is the radius of the particle, β is the aspect ratio of the cylindrical particle, δ is the average thickness of liquid coating the particle, ρ_p is the particle density, ρ_l is the liquid density, and ε_o is the vacuum permittivity. The model was tested for spherical particles ranging from approximately 800 μm to 1.6 mm in diameter, and for cylindrical particles ranging from approximately 100 μm to 300 μm in diameter with aspect ratios ranging from 5 to 15.

Particles smaller than the these ranges could not be extracted because they require an extraction electric field that exceeds the electric field required to initiate an instability on the liquid surface. The minimum electric field required to initiate an instability on an unperturbed liquid surface was first analyzed by Tonks's[8], and was re-derived recently to be[7]

$$E_{liq,thresh} = C_e^{1/4}\left(\frac{\gamma\rho_\ell g}{\varepsilon_o^2}\right)^{1/4}\ , \tag{3}$$

where C_e is a constant whose value lies between 1.34 and 4.5.

Before proceeding further, it is important to note that the extraction and charging electric fields are coupled together and the relationship between the two is determined by the boundary condition between the dielectric liquid and air/vacuum, which can be expressed as

$$\varepsilon_o E_{ex} = \varepsilon_\ell E_{ch}\ , \tag{4}$$

when there is no net charge on the liquid surface. Therefore, both the charging and extraction electric field strengths are limited by the liquid instability. If the charging and extraction electric fields were decoupled, the extraction electric field would still be limited by the liquid instability, but the charging electric field would not. The electrical breakdown of the dielectric liquid would provide the upper limit for the charging electric field, which is typically at least an order of magnitude higher than the liquid instability threshold. For example, silicone oil will breakdown under a charging electric field of approximately 15 MV/m,[9] but it will be become unstable under an extraction electric field of approximately 1.3 to 1.8 MV/m, according to Equation (3). Therefore, decoupling the charging and extraction electric fields will allow approximately another order of magnitude of charge to be placed on the particle, while using the same strength extraction electric field, which should allow for the extraction of much smaller particles.

The method to decouple the charging and extraction electric fields is to insert a third electrode into the extractor system, level with the liquid surface, as shown in Figure 7.

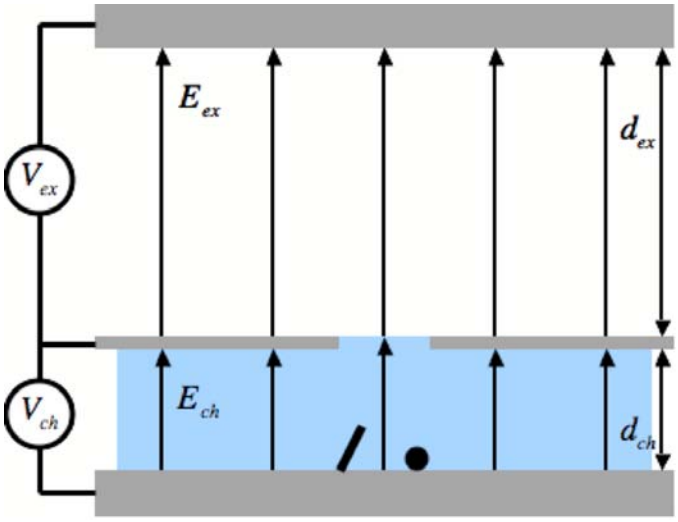

Figure 7: Experimental setup for particle extraction from insulating liquid when decoupling the charging and extraction electric fields.

Now, the charging electric field is controlled by the charging voltage, V_{ch}, and the dimensions of the liquid gap, while the extraction electric field is controlled by the extraction voltage, V_{ex}, and the dimensions of the air/vacuum gap. The extraction and charging electric fields can be approximated as

$$E_{ex} = \frac{V_{ex}}{d_{ex}} \quad (5) \qquad \text{and} \qquad E_{ch} = \frac{V_{ch}}{d_{ch}}, \quad (6)$$

respectively, as long as the diameter of the channel in the middle electrode is less than or equal to both electrode gaps, d_{ex} and d_{ch}.[10] The minimum extraction electric field required to achieve particle extraction when decoupling the charging and extraction electric fields was derived for spherical and cylindrical particles to be[7]

$$E_{ex,thresh,sph} = \frac{3\gamma(r+\delta) + g\left[(r+\delta)^3\rho_\ell + 2r^3(\rho_p - \rho_\ell)\right]}{\pi^2 r^2 \varepsilon_\ell E_{ch}} \quad \text{and} \quad (7)$$

$$E_{ex,thresh,cyl} = \frac{\left[\gamma(r+\delta) + g\beta\left\{r^3\rho_p - \rho_\ell\left(r^3 - \frac{(r+\delta)^3}{2\beta}\right)\right\}\right]\left[\ln(4\beta) - 1\right]}{2r^2\beta^2\varepsilon_\ell E_{ch}}, \text{ respectively.} \quad (8)$$

Since there is theoretically a significant advantage to using a charging grid to decouple the charging and extraction electric fields, we have designed and fabricated a prototype emitter that utilizes a charging grid level with the liquid surface. The advanced microparticle emitter prototype was designed to charge, extract, accelerate, and eject particles ranging from a few microns up to a few millimeters, but is intended to focus on particles in the 1 μm to 50 μm diameter range.

The main goals of the prototype are to demonstrate a functional microparticle emitter system operating with particles in the micron range, prove the feasibility of extracting micron sized particles from an insulating liquid, and to verify the particle extraction models. In addition to further developing the nanoFET concept, we will study the effects of impacting high energy microparticles on various materials to learn more about using nanoFET for biomedical, material processing, and printing applications. The design of the prototype system is discussed in the next section.

B. Design of the Microparticle Emitter Prototype

The microparticle emitter prototype was designed to charge, extract, accelerate, and eject particles ranging from a few microns to a few millimeters in diameter using an array of 100 emitters. The target goal of emitting micron sized particles with this device is the next step in the process of scaling the particle size from the initial millimeter sized particles down to the final nanometer sized particles, and to allow for the development of the particle extraction physics as the particle size is reduced.

Figure 8 is a schematic showing the cross-sectional view of a single emitter used in this prototype.

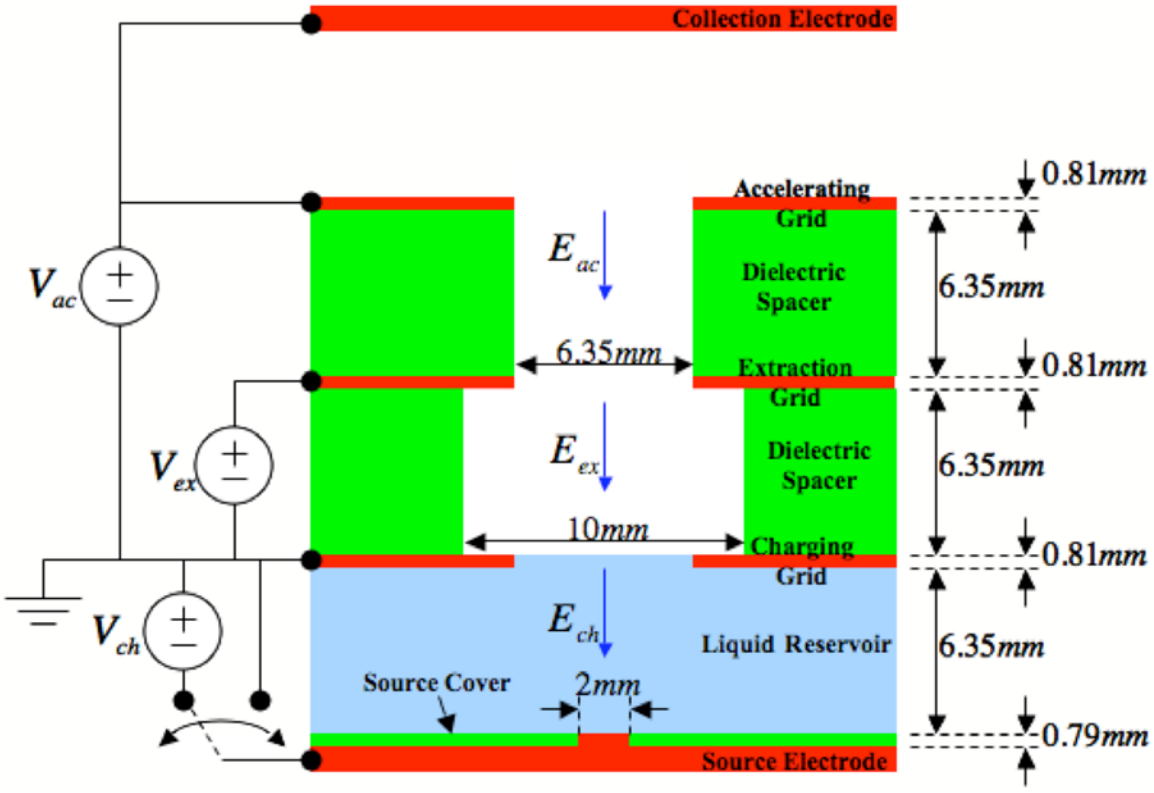

Figure 8: Schematic showing the cross-sectional view of a single emitter used in the first generation microparticle emitter prototype.

The prototype uses five stacked electrodes made from aluminum spaced 6.35 mm apart. The bottom electrode, termed the source electrode, is biased negatively and is the source of electrons to charge the particles. A short 2 mm diameter pad is milled in the source electrode centered just beneath the acceleration channel and is the location for particle charging. A source cover made from 0.79 mm thick Teflon covers the source electrode except for the protruding charging pad. This assures that particles are only charged when centered and beneath the acceleration channel in contact with the pad so that the particles are only extracted and accelerated down the center of the channel to reduce particle impingement on the grids and to decrease the expected cosine efficiency loss due to a poorly collimated particle beam.

The second electrode, termed the charging grid, is grounded and fixed at a height of 6.35 mm above the source electrode and level with the liquid surface. The electric potential between the source electrode and the charging grid produces the charging electric field in the liquid reservoir. A 6.35 mm hole is drilled in the charging grid to allow for the passage of particles.

The third electrode, termed the extraction grid, is biased positively and placed at a height of 6.35 mm above the charging grid and is responsible for generating the extraction electric field. The gap between the charging and extraction grids is maintained with a 6.35 mm thick Teflon spacer. Teflon was chosen as the spacer material due to its low electrical conductivity and high electrical breakdown properties. Note that the diameter of the hole in this

Teflon spacer is 10 mm, which is larger than the rest of the acceleration channel. This large hole is used to prevent the liquid from capillary climbing out of the liquid reservoir and up the entire acceleration channel.

The fourth electrode, termed the acceleration grid, is biased positively at a value greater than the extraction grid and placed at a height of 6.35 mm above the extraction grid. As indicated by its name, this grid is responsible for additional acceleration of the charged particles. Again, a Teflon spacer is used to maintain the gap between the extraction and accelerating grids, but unlike the first Teflon spacer, the hole has the same diameter as the rest of the acceleration channel. It is important to understand that additional acceleration grids can be stacked on top of the one shown if a greater potential drop for particle acceleration is needed.

The fifth electrode, termed the collection electrode, is generally electrically connected to the top acceleration grid and placed above it in order to collect all ejected particles. By electrically connecting the collection plate to the acceleration grid, no electric fields should be generated in the gap between the top acceleration grid and the collection electrode. Therefore, ejected particles will experience only the gravitational force and air resistance, and the ejected particles's velocities can be determined using various diagnostics.

Several high voltage power supplies are required to operate the prototype with the exact number dependant on the number of accelerating grids. All power supplies are grounded to the charging grid and their high voltage outputs are connected to their respective grids. A negatively biased power supply is used for the source electrode while positively biased power supplies are used for the extraction and accelerating grids to emit negatively biased particles. It is possible to reverse the polarity of all the power supplies to emit positively charged particles.

The entire prototype consists of an array of 100 emitters organized in a 10 by 10 square pattern and mounted in a bath structure used to regulate the height of the liquid, as shown in Figure 9. Five alignment pins made from Ultem, an insulating material, are used to keep all of the grids and spacers properly aligned. Extending off of each electrode is a thin aluminum tab that provides a safe means for the high voltage connections.

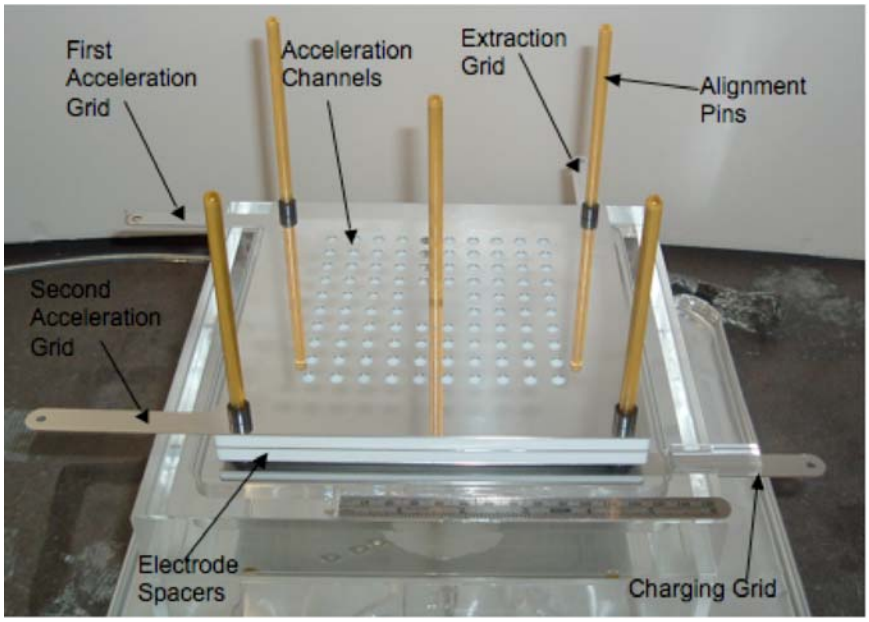

Figure 9: Picture of the first generation microparticle emitter prototype used to charge, extract, accelerate, and eject micron sized particles.

To operate the prototype, the conducting particles are loaded into the liquid reservoir prior to the assembly of the grid structure. Once the particles and liquid are situated, the grids and spacers are stacked as desired and the high voltage power supplies are connected appropriately. The positively biased power supplies connected to the extraction and accelerating grids are powered up and set to the desired potentials. Note that the negatively biased power supply connected to the source electrode is connected through a high voltage switch, which is controlled by a high voltage relay. This power supply is powered up with the switch connected to ground so that the charging electric field remains zero until the operator wishes to "turn on" the prototype. When ready, the switch is thrown to connect the high voltage to the source electrode, which allows the charging electric field in the liquid reservoir to be turned on almost instantly.

It should be noted that this generation of the prototype uses a shotgun method where the particles need to be loaded into the reservoir manually each time. A future generation will implement a particle delivery system so that the prototype can operate continuously.

C. Results from the Microparticle Emitter Prototype Extraction Tests

As previously stated, the main goals of this prototype are to demonstrate a functional microparticle emitter system operating with particles in the micron range, to prove the feasibility of extracting micron sized particles from an insulating liquid, and to verify the particle extraction models for both spherical and cylindrical particles. Previous particle extraction tests that utilized a duel electrode extraction system, like the one in Figure 6 without a charging grid to decouple the charging and extraction electric fields, successfully demonstrated particle extraction for both spheres and cylinders in the many hundreds of microns to millimeter range.

To initiate testing with the prototype, we began by extracting aluminum spheres with diameters of 1.6 mm and 800 μm from 50 cSt silicone oil and measured the minimum extraction electric field required to achieve particle extraction. The 50 cSt silicone oil has a surface tension of 0.0208 N/m, a density of 963 kg/m^3, and a relative dielectric constant of 1.97;[11] the aluminum particles have a density of 2,700 kg/m^3. When considering the liquid instability threshold, shown in Equation (3), for comparison to the required extraction electric field, we chose to set the constant C_e equal to 1.34 in order to give a worst-case scenario.

Figure 10 shows a plot of the theoretical threshold extraction and threshold liquid instability electric fields when extracting these aluminum spherical particles from the 50 cSt silicone oil using the prototype with a charging electric field of 1.5 MV/m. Also included in the plot are the minimum measured extraction electric fields to achieve particle extraction for both particle sizes. The theoretical minimum extraction electric field (solid blue line) is obtained when the average thickness of liquid coating the particle during extraction is set to zero. And, the theoretical maximum extraction electric field (dashed purple line) is obtained when the average thickness of liquid coating the particle is assumed to be equal to the particle radius. This approximation was determined by solving the viscous flow problem for liquid draining from the particle assuming that the particle was extracted at terminal velocity and is in laminar flow. The discussion of liquid draining from the particle is beyond the scope of this paper, but will be addressed in a future publication.

Note that theoretical prediction for particle extraction can be divided into two regimes. When the particle size is reduced below the millimeter range, the required extraction electric field increases as particle size decreases due to the surface tension of the liquid. When the particle size is increased above the millimeter range, the required extraction electric field increases as particle size increases due to gravity.

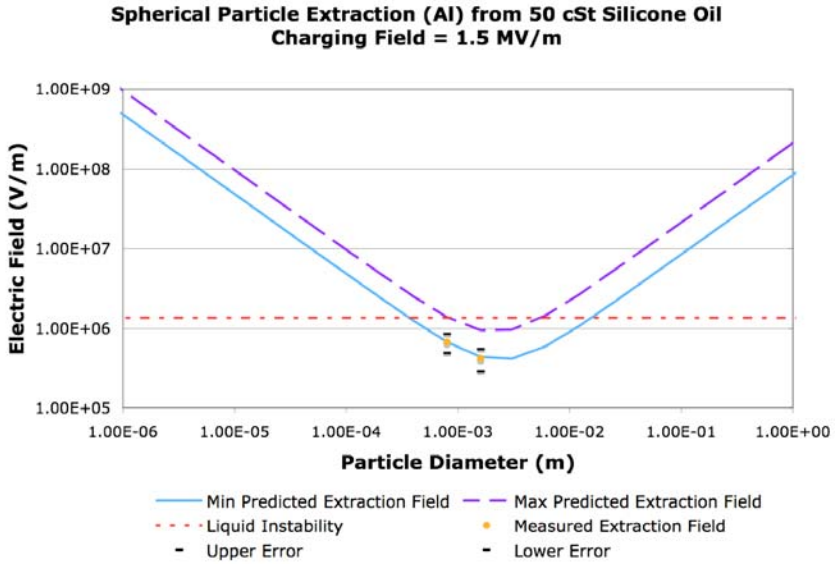

Figure 10: Plot of the theoretical threshold extraction and threshold instability electric fields when extracting aluminum spherical particles from 50 cSt silicone oil using a charging electric field of 1.5 MV/m along with experimental results.

The plot in Figure 10 shows that the two experimental data points agree very well with the minimum expected particle extraction electric field, which suggests that the spherical particle extraction model is reasonably accurate for particles in this size range. According to high speed video of the particle extraction, the thickness of liquid coating the particle is much less than the radius of the particle.

To scale down the particle size, we continued by extracting spherical particles made from a 95% Sn and 5% Sb alloy with a diameter of 508 μm from 50 cSt silicone oil and measured the minimum extraction electric field required to achieve particle extraction. The 95Sn/5Sb alloy has a density of 7,279 kg/m^3. Figure 11 shows a plot of the theoretical threshold extraction and threshold liquid instability electric fields when extracting these spherical particles from the 50 cSt silicone oil using the prototype with a charging electric field of 1.8 MV/m. Also included in the plot is the minimum measured extraction electric field to achieve particle extraction for this particle size.

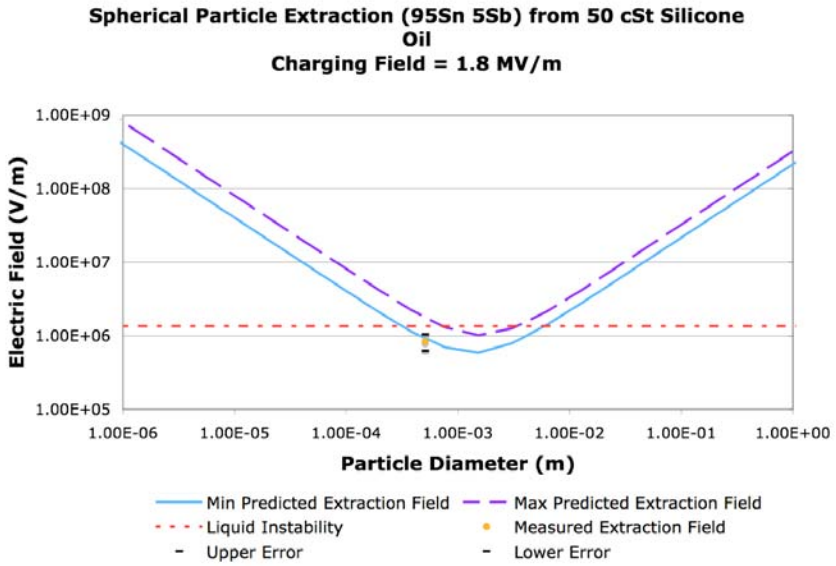

Figure 11: Plot of the expected threshold extraction and threshold instability electric fields when extracting 95Sn/5Sb spherical particles from 50 cSt silicone oil using a charging electric field of 1.8 MV/m along with experimental results.

The plot in Figure 11 shows that the experimental data point agrees very well with the minimum expected particle extraction electric field, which suggests that the spherical particle extraction model is reasonably accurate for particles down to this scale. Unfortunately, we were unable extract spherical particles below this scale without inducing an instability in the liquid surface. It is probable that smaller spherical particles are extractable if a higher strength charging electric field were used, but for this experiment the charging electric field was limited to 1.8 MV/m.

To initiate testing cylindrical particle extraction with the prototype, we began by extracting aluminum cylinders with a diameter of 300 μm and an aspect ratio of 6.67 from 50 cSt silicone oil and measured the minimum extraction electric field required to achieve particle extraction.

Figure 12 shows a plot of the theoretical threshold extraction and threshold liquid instability electric fields when extracting these cylindrical particles from the 50 cSt silicone oil using the prototype with a charging electric field of 1.5 MV/m. Also included in the plot is the minimum measured extraction electric field to achieve particle extraction for this particle size.

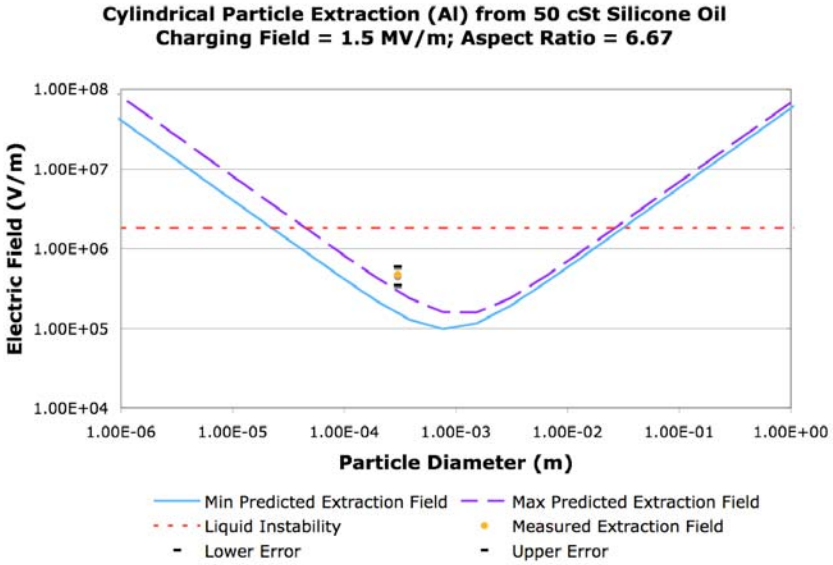

Figure 12: Plot of the expected threshold extraction and threshold instability electric fields when extracting aluminum cylindrical particles with an aspect ratio of 6.67 from 50 cSt silicone oil using a charging electric field of 1.5 MV/m along with experimental results.

The plot in Figure 12 shows that the cylindrical particle extraction model underestimates the minimum extraction electric field required to achieve particle extraction for this particle size by a factor of approximately 1.6. Potential reasons for this discrepancy are discussed in the next section.

To scale down the particle size, we continued by extracting cylindrical particles made from tungsten with diameters of 152, 102, and 50.8 μm and an aspect ratio of 13 from 50 cSt silicone oil and measured the minimum extraction electric field required to achieve particle extraction. The tungsten particles have a density of 19,250 kg/m^3. Figure 13 shows a plot of the theoretical threshold extraction and threshold liquid instability electric fields when extracting these cylindrical particles from the 50 cSt silicone oil using the prototype with a charging electric field of 1.5 MV/m. Also included in the plot is the minimum measured extraction electric field to achieve particle extraction for these particle sizes.

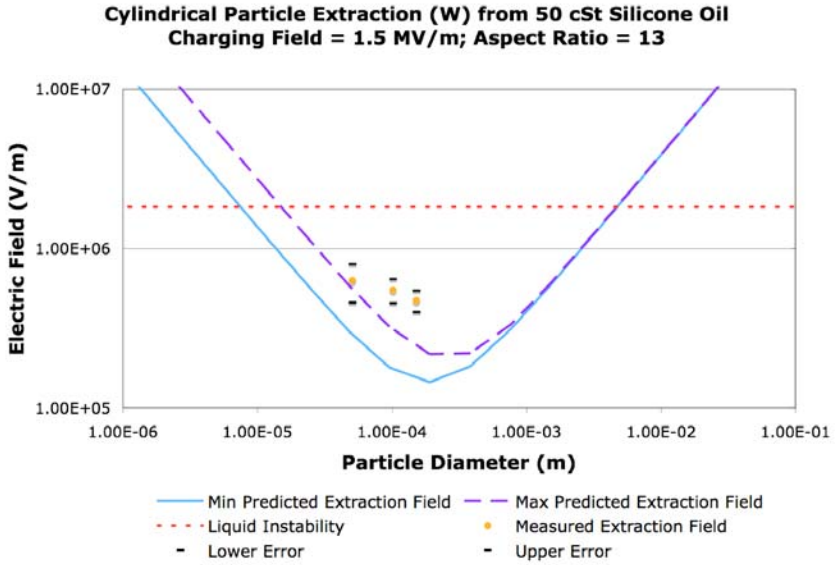

Figure 13: Plot of the expected threshold extraction and threshold instability electric fields when extracting tungsten cylindrical particles with an aspect ratio if 13 from 50 cSt silicone oil using a charging electric field of 1.5 MV/m along with experimental results.

The plot in Figure 13 shows that the cylindrical particle extraction model also underestimates the minimum extraction electric fields required to achieve particle extraction for cylinders as the diameter is reduced from approximately 150 μm down to 50 μm by factors of approximately 2 to 1.1, respectively.

To scale down the particle size further, we continued by extracting tungsten cylindrical particles with a diameter of 25.4 μm and an aspect ratio of approximately 60 from 50 cSt silicone oil and measured the minimum extraction electric field required to achieve particle extraction. Figure 14 shows a plot of the theoretical threshold extraction and threshold liquid instability electric fields when extracting these cylindrical particles from the 50 cSt silicone using the prototype with a charging electric field of 1.5 MV/m. Also included in the plot is the minimum measured extraction electric field to achieve particle extraction for this particle size.

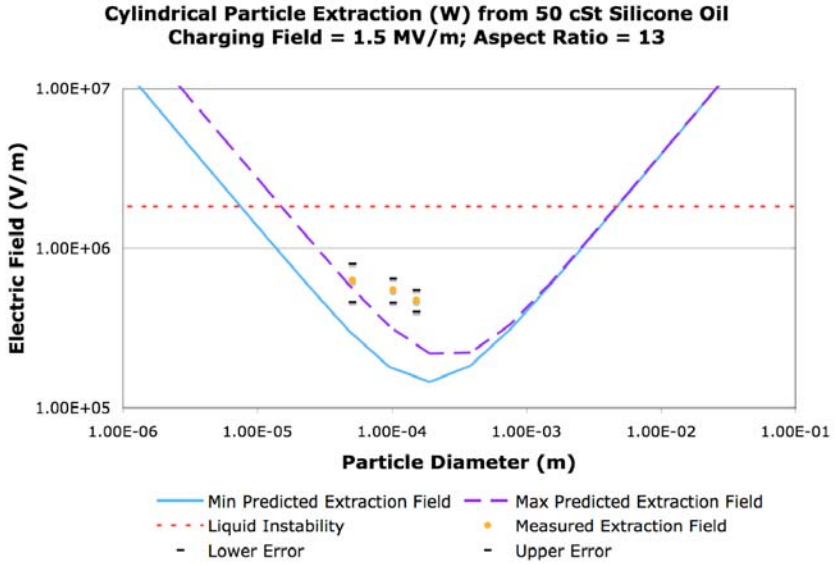

Figure 14: Plot of the expected threshold extraction and threshold instability electric fields when extracting tungsten cylindrical particles with an aspect ratio if 60 from 50 cSt silicone oil using a charging electric field of 1.5 MV/m along with experimental results.

The plot in Figure 14 shows that the cylindrical particle extraction model continues to underestimate the minimum extraction electric field required to achieve particle extraction for cylinders as the diameter is reduced to approximately 25 μm by a factor of approximately 2.

The experimental data collected from the spherical and cylindrical particle extraction tests when using the first generation microparticle emitter prototype proved the feasibility of extracting charged spheres ranging in diameter from 1.6 mm down to 508 μm and cylinders ranging from 300 μm down to 25.4 μm. For the particle ranges studied, we found that the spherical particle extraction model predicted the minimum required extraction electric field very accurately. The cylindrical particle extraction model tended to underestimate minimum required extraction electric field by upwards of a factor of two. Based on the particle extraction tests, we strongly believe that it is possible to continue scaling down the particle size and still achieve particle extraction.

D. Potential Problems with the Microparticle Emitter Prototype

The previous section presented experimental data collected for the minimum extraction electric fields required for both spherical and cylindrical particles. The data suggests that the spherical particle extraction model accurately predicted the minimum extraction electric fields for the successfully extracted particles ranging from as large as 1.6 mm down to approximately 500 μm. But, the data also suggests that the cylindrical particle extraction model under predicts the minimum extraction electric fields for the successfully extracted cylinders with diameters ranging from 300 μm down to 25 μm.

When measuring the minimum required extraction electric fields for the cylindrical particles, we found that the particles were extracted with a very low probability when the extraction electric field was close to the minimum required values. When the extraction electric field was increased significantly above the minimum values, we found that the probability of achieving particle extraction increased. This section discusses several potential problems with the first generation prototype that may limit the probability of achieving particle extraction.

Figure 15 depicts a typical progression of a cylindrical particle that is not successfully extracted through the liquid surface when the liquid level is even with the charging grid based on an analysis of high speed video. The particle is initially charged on the exposed surface of the source electrode (diagram a). Once sufficiently charged, the particle is transported to the liquid surface by the charging electric field (diagram b). When at the liquid surface, the particle experiences a significant deceleration due to the surface tension resisting the extraction of the particle. If the particle is not exactly on the channel centerline, the low strength radial electric fields begin to rotate and move it towards the charging grid (diagram c). Once the particle begins to rotate, it appears that it is inevitable that the particle will crash into the charging grid and undergo a charge exchange ending the possibility of achieving particle extraction (diagram d).

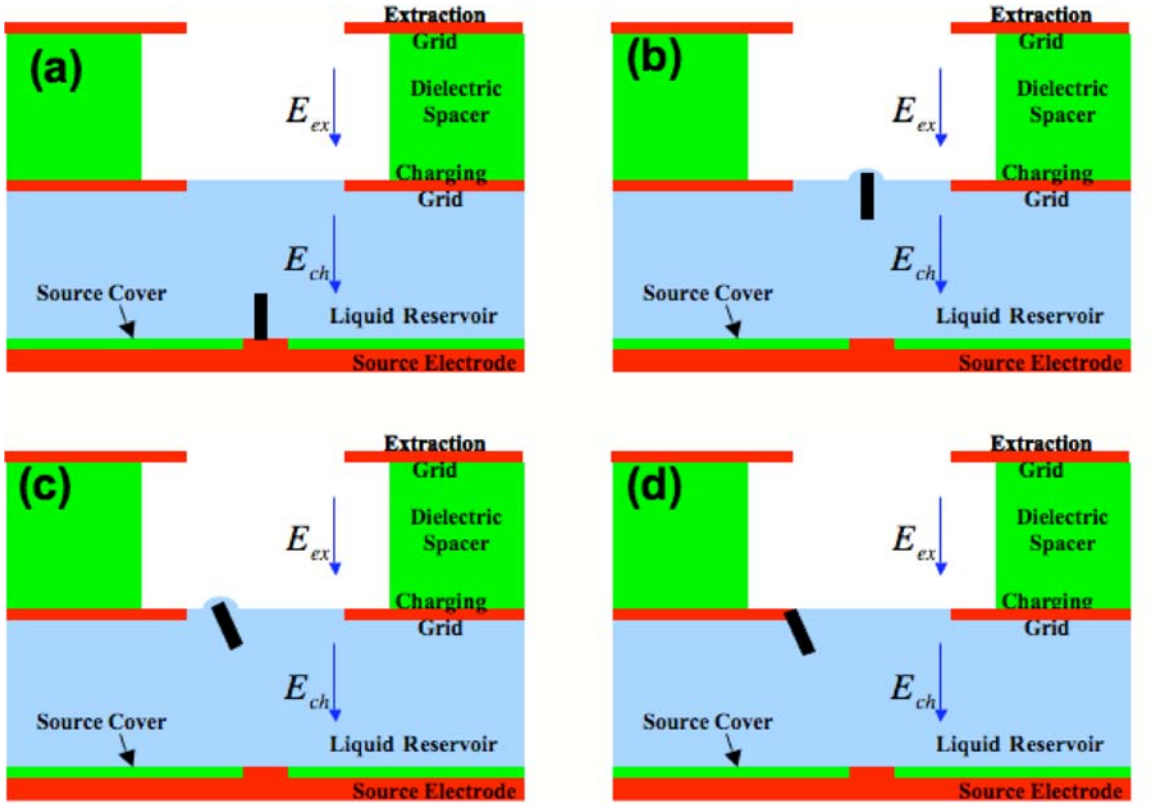

Figure 15: Typical progression of an unsuccessfully extracted cylindrical particle. (a): Particle is charged on exposed source electrode. (b): Particle transported to liquid surface and decelerated by surface tension. (c): Radial electric fields rotate particle and pull it towards charging grid. (d): Particle crashes into charging grid and undergoes a charge exchange to end possibility of particle extraction.

There are several issues with the first generation microparticle emitter prototype that could lead to the low probability of particle extraction when the minimum required extraction electric field is exceeded.

- *Radial Electric Fields the at the Particle Extraction Point*

  When designing the first generation microparticle emitter prototype, we used the rule of thumb that if the ratio of the electrode gap to the diameter of the acceleration channel is greater than or equal to one, then the electric fields will be predominantly in the axial direction.[10] But, we know that there will exist some electric fields in the radial direction as illustrated in the multi-grid structure in Figure 11, which was simulated using COMSOL Multiphysics™, a finite element analysis and solver software package for various physics and engineering applications, with electrode gaps and an acceleration channel diameter of 6.35 mm. Note that the radial component of the electric field is strongest near the corners of the grid structures due to field focusing.

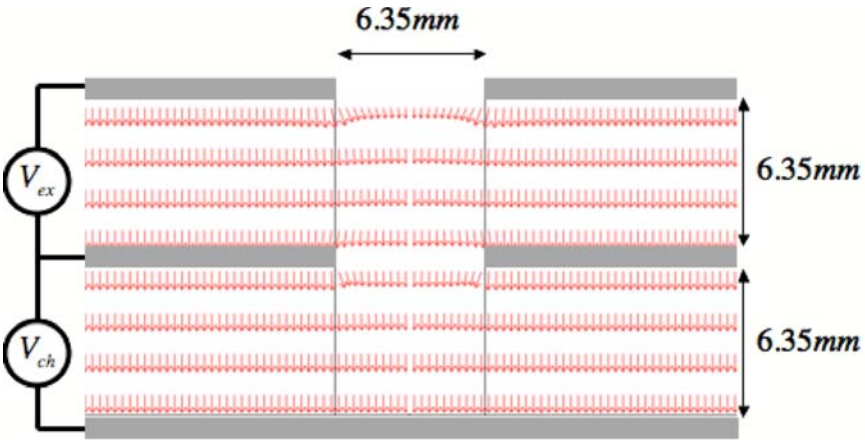

Figure 16: Simulation showing direction of electric field in multi-grid structure when using ratio of electrode gap to channel diameter of one.

We also know from analyzing high speed video of particle extraction, that the particle experiences a significant deceleration during the extraction process. Therefore, if a particle is brought to the liquid surface and is not centered in the channel, its momentum may not be sufficient to escape the electrical force supplied by the radial fields. As a result, the particle can be pulled horizontally and into the charging grid as shown in Figure 15.

- *Particles not Completely Charged*

  It is also possible that the particles are not charged to the level predicted by Felici's model.[12] Experiments, which will be discussed in a future publication, suggest that an inadequate electrical contact between the source electrode and the particle will limit the rate at which the particles can be charged. Experimental results suggest that under high strength electric fields, the charging time of the particles may be longer than the time that the particles will remain in contact with the source electrode due to the thin layer of high resistance oxide that can form on the surface of certain particles and the source electrode.

  If the particles are not completely charged, then the electrical force from the extraction electric field attempting to pull the charged particles from the liquid is less than predicted by the particle extraction model and a stronger extraction electric field will be required.

- *Particles not Arriving at the Liquid Surface Completely Vertical*

  It has been witnessed that most cylindrical particles, when transported through the liquid, arrive at the liquid surface oriented a few degrees off vertical. If a particle arrives at the liquid surface off vertical, then its exposed area increases and the force from the surface tension, which resists extraction, increases. The surface tension force is defined as[13]

$$F_s = \left(\frac{2\gamma}{R}\right)A, \tag{9}$$

  where γ is the surface tension of the liquid, R is the radius of the liquid perturbation, and A is the exposed area of the particle. When the surface tension force increases, then a stronger extraction electric field is required for particle extraction.

It is possible that these three issues could significantly limit the probability of achieving particle extraction when operating at or slightly above the predicted extraction electric field strengths. The next section briefly discusses ideas to help alleviate these issues that can be addressed in the future generations of the microparticle emitter prototype.

E. Possible Improvements to Microparticle Emitter Prototype

The previous section presented issues with the first generation microparticle emitter prototype that could be reasons for the low probability of achieving particle extraction when operating at or slightly above the predicted minimum extraction electric fields. This section will discuss possible solutions to a couple of these issues that can be implemented in future generations.

- *Increase Height of Liquid Surface to Reduce Radial Electric Fields at Extraction Point*

  The previous section discussed that since the particles experience a significant deceleration during the extraction process at the liquid surface due to the surface tension, low strength radial electric fields can pull the particle in the radial direction resulting in the particle crashing into the charging grid as shown in Figure 15. Since the first generation prototype placed the charging grid even with the liquid surface as shown in Figure 8, the radial electric fields are strongest at the liquid surface where the deceleration occurs. If the liquid height was changed to a location where the radial electric fields were minimal, it is possible that the particles would have sufficient time for extraction before being pulled significantly in the radial direction.

  According to the simulation in Figure 16, the radial electric fields are minimized at the midpoint between the grid structures. Therefore, we expect that this problem may be reduced if the liquid surface were raised above the charging grid and held at the midpoint between the charging and extraction grids as shown in Figure 17.

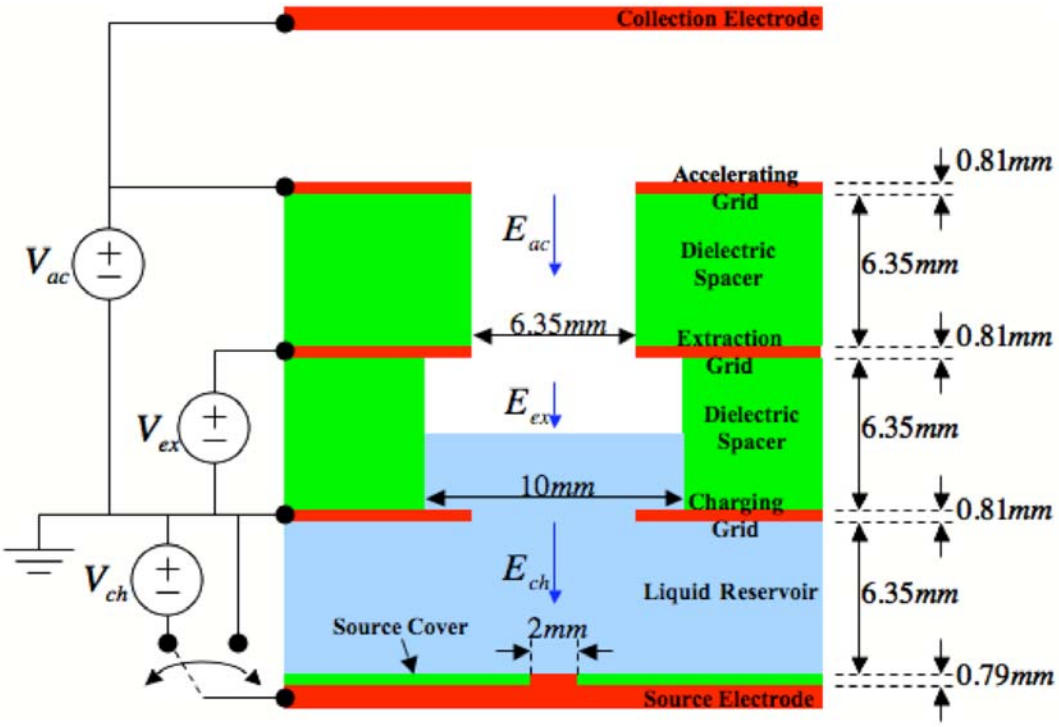

Figure 17: schematic showing the cross-sectional view of a single emitter for a future generation prototype with liquid surface between charging and extraction grids to reduce radial electric fields at extraction point.

- *Use Non-Oxidizing Materials for Particles and Source Electrode*

  It was suggested in a previous section that the thin oxide that forms on the surface of some metallic materials might limit electrical contact between the particles and the source electrode during the particle charging process. Current models and experimental results suggest that this might increase the charging time of the particles to a point where they are not fully charged before being lifted from the source electrode. The first generation prototype implemented a source electrode fabricated from aluminum, which forms a thin aluminum oxide layer with a thickness of approximately 4 nm.[14]

To reduce the charging time of the particles and to assure that they are completely charged, a future generation of the prototype may fabricate the source electrode from a non-oxidizing material or coat the electrode with a non-oxidizing material such as gold.

III. Conclusion

The development of the first generation microparticle emitter prototype has allowed us to begin experimentally testing particle extraction for both spheres and cylinders when using a charging grid level with the liquid surface to decouple the charging and extraction electric fields. Decoupling these electric fields makes it possible to begin scaling down the particle size. The experimental data collected from the spherical and cylindrical particle extraction tests prove the feasibility of extracting charged spheres ranging in diameter from 1.6 mm down 508 μm and cylinders ranging from 300 μm down to 25.4 μm. For the particle ranges studied, we found that the spherical particle extraction model predicted the minimum required extraction electric field very accurately. The cylindrical particle extraction model tended to underestimate minimum required extraction electric field by upwards of a factor of two. Based on the particle extraction tests, we strongly believe that it is possible to continue scaling down the particle size and still achieve particle extraction.

Acknowledgments

This project is funded by a Phase 2 grant (NAS5-03110) from the NASA Institute for Advanced Concepts (NIAC). Thanks to Jason Marron at Bucknell University for generating the plot in Figure 16, and Bailo Ngom from the University of Michigan Plasmadynamics and Electric Propulsion Laboratory for his help with Figure 1. Thanks also to Steven Morris and Liang Tao at the University of Michigan for their contributions.

References

[1] Musinski, L., Liu, T., Gilchrist, B., Gallimore, A., and Keidar, M., "Scalable Flat-Panel Nano-Particle MEMS/NEMS Thruster." International Electric Propulsion Conference (IEPC), Princeton, NJ, October 31 – November 4, 2005.

[2] Musinski, L., Liu, T., Gilchrist, B., Gallimore, A., and Keidar, M., "Nanoparticle Electric Propulsion: Experimental Results." AIAA-2006-4803, 42nd AIAA/ASME/SAE/ASEE Joint Propulsion Conference and Exhibit, Sacramento, CA, July 9-12, 2006.

[3] Behan, Niall, "Nanomedicin and Drug delivery at the University of Limerick," The University of Limerick. http://www.ul.ie/elements/Issue4/behan.htm

[4] Liu, T., Keidar, M., Musinski, L., Gallimore, A., and Gilchrist, B., "Theoretical Aspects of Nanoparticle Electric Propulsion." AIAA-2006-4335, 42nd AIAA/ASME/SAE/ASEE Joint Propulsion Conference and Exhibit, Sacramento, CA, July 9-12, 2006.

[5] Liu, T., Musinski, L., Patel, P., Gallimore, A., Gilchrist, B., and Keidar, M., "Nanoparticle Electric Propulsion for Space Exploration." Space Technology and Applications International Forum (STAIF), Albuquerque, NM, February 11-15, 2007.

[6] Wertz, Larson, "Space Mission Analysis and Design 3rd Ed." 1999.

[7] Musinski, L., Liu, T., Gilchrist, B., Gallimore, A., and Keidar, M., "Experimental Results and Modeling Advances in the Study of Nanoparticle Field Extraction Thruster." AIAA-2007-5254, 43rd AIAA/ASME/SAE/ASEE Joint Propulsion Conference & Exhibit, Cincinnati, OH, July 8-11, 2007.

[8] Tonks, L., "A Theory of Liquid Surface Rupture by a Uniform Electric Field," *Physical Review*, Vol. 48, 15 September 1935, pp. 562-8.

[9] Elert, G., "The Physics Hypertextbook," 1998-2007, http://hypertextbook.com/physics/

[10] Goldberg, H., Encarnacion, P., Morris, D., Gilchrist, B.,Clarke, R., "Cold-Cathode Electron Field Emission of Boron Nitride Thin Film with a MEMS-Based Gate for Space Applications." AIAA-2004-3499, 40th AIAA/ASME/SAE/ASEE Joint Propulsion Conference & Exhibit, Fort Lauderdale, FL, July 11-14, 2004.

[11] "Clearco Pure Silicone Fluids: Product Information." Clearco Products Co., Inc. Bensalem, PA 19020

[12] Felici, N. Rev. Gen. Elect., 75, pp. 1145-1160, 1966.

[13] Wilkes, J., "Fluid Mechanics for Chemical Engineers," Prentice Hall International Series, 1999, p 16.

[14] Tamura, K., Kimura, Y., Suzuki, H., Kido, O., Sato, T., Tanigaki, T. "Structure and Thickness of Natural Oxide Layer Ultrafine Particles." Journal of Applied Physics, 2003, Vol 42, pp 7489-7492.